BNL-226014-2024-JAAM

Developing Benzodithiophene-Free donor polymer for 19.36% efficiency Green-Solvent-Processable organic solar cells

Y. He, R. Li

To be published in "Chemical Engineering Journal"

June 2024

Photon Sciences

Brookhaven National Laboratory

U.S. Department of Energy

USDOE Office of Science (SC), Basic Energy Sciences (BES)

DISCLAIMER

Developing Benzodithiophene-Free Donor Polymer for 19.36% Efficiency Green-Solvent-Processable Organic Solar Cells

Ying He,[a] Wenwen Jing,[a] Chentong Liao,[a] Xiaopeng Xu,[a] Yuwei Duan,[b] Ruipeng Li,[c] Liyang Yu,[a] Qiang Peng*[a]*

[a] School of Chemical Engineering and State Key Laboratory of Polymer Materials Engineering, Sichuan University, Chengdu 610065, P. R. China.

[b] College of Materials and Chemistry & Chemical Engineering, Chengdu University of Technology, Chengdu 610059, P. R. China.

[c] National Synchrotron Light Source II Brookhaven National Lab, Suffolk, Upton, NY 11973, USA

*To whom correspondence should be addressed: Tel: +86-28-86510868; fax: +86-28-86510868; e-mail: xpxu@scu.edu.cn; qiangpeng@scu.edu.cn

Abstract

In this work, a newly benzodithiophene-free D-A polymer donor, named PDTP-BDD, was developed for realizing green-solvent processed high-performance OSCs. By bridging two electron-rich unit of dithieno[3,2-b:2′,3′-d]pyridin-5(4H)-one (DTP) and electron-deficient benzo[1,2-c:4,5c′]dithiophene-4,8-dione (BDD) with thiophene units, PDTP-BDD possesses high absorption in the short wavelength range and a deep HOMO energy level. The rigid building blocks also make PDTP-BDD has strong aggregation and poor solubility in common halogen-free solvents (such as *o*-xylene) at room temperature, but it is readily dissolved and disaggregated at high temperature (120 ºC). After cooling down to a lower temperature (60 ºC), PDTP-BDD self-assembled and pre-aggregated slowly in the solution at a long time. By employing a delayed processing strategy in the layer-by-layer processed OSCs (LbL-OSCs), an optimized fibril network of the underling layer was realized, enabling the permeation of acceptor into the donor network. The optimized PDTP-BDD/L8-BO-based LbL-OSCs realized a high PCE of 18.42%. By adding a small amount of D18 to further optimize the PDTP-BDD fibril network, an impressive PCE of 19.36% was achieved finally in the resulting ternary LbL-OSCs, which is the highest value for OSCs processed by halogen-free solvents.

Keywords: organic solar cells, green solvent aging, layer-by-layer processing, morphology optimization, fibrous-network structure

1. Introduction

Organic solar cells (OSCs) are recognized as a promising and versatile off-grid energy supply candidate for portable devices, wearable electronic devices and internet-of-things (IoT) integrated devices in the future.[1-4] Over the past years, great efforts have been devoted to new materials design and devices engineering, which continuously improve the photovoltaic

performance of OSCs.[5] Especially, the great success of nonfullerene acceptors (NFAs) with largely improved absorption in the near-infrared (NIR) region has put the power conversion efficiency (PCE) of OSCs over 19%, showing great potential for practical applications.[6-18] In contrast to the explosive growth of efficient NFAs, the development of matched high performance polymer donors lags relatively behind and is of great need to further improve the device efficiency of OSCs.

With regard to the polymer donor development, it has become a design paradigm to adopt the donor-acceptor (D-A) alternating structure, in which an electron-rich unit and electron poor unit are connected without or with π-bridges.[19, 20] By rationally choosing D and A units to regulate the "push-pull" effect, the absorption and energy levels of the D-A copolymers can be readily modulated, enabling them to match well with diversified NFAs for realizing high-performances. So far, the most efficient polymer donors are based on the D-A structure, such as PM6, D18, PTQ10, PBTZ-F, QQ1, PBBTz-Cl *etc*.[6, 21-25] However, the further development of D-A copolymers is severally restrained by the limited number of efficient donor blocks, especially the donor blocks for wide bandgap (WBG) polymer donors. The currently high-performance WBG polymers still mainly rely on the benzodithiophene (BDT) donor block due to its weak electron donating ability and rigid coplanar structure, as well as the easily modulated side chains.[26, 27] The limited selection of donor blocks seriously restricts the diversification of the WBG polymer donor materials. The development of BDT-free polymer donors still lags far behind so far, the underlying design principle and application potential of BDT-free polymers remain to be better understood.

In addition to the material design, the delicate morphology control also plays a vital role in improving the device performances of OSCs. The prevailing OSCs typically comprise a bulk-heterojunction (BHJ) photoactive layer, where an ideal bicontinuous interpenetrating network formed by the spontaneous phase separation of premixed donor and acceptor materials is crucial for efficient exciton dissociation and charge transport.[28-31] Therefore, it is critically important

to develop proper strategies to optimize the morphology based on the unique properties of donor and acceptor materials.[32] To meet the solution processing requirement, an appropriate solvent is needed to dissolve the photoactive materials. Due to their excellent dissolvability, halogenated solvents, such as chloroform (CF) and chlorobenzene (CB), are mostly employed to process the photoactive layer. However, halogenated solvents are detrimental to the environment and our health, thus not adaptable for practical mass production.[33] To circumvent the disadvantages of halogenated solvents, more and more attention is paid to employing halogen-free or green solvents to process the photoactive layer.[34-41] The main issue limiting the widespread use of halogen-free or green solvents is their relatively low dissolvability to the majority of donor and acceptor materials, because of the extended π-conjugation, strong intermolecular aggregation and high molecular weight. To realize halogen-free or green solvent processability, hot-spin coating was developed, where the over aggregation of photoactive materials could be prevented by elevating the temperature and thus improved solubility.[41-43] In the hot spin-coating procedure, the pre-aggregation of photoactive materials is highly sensitive to the temperature of both the solution and substrates. Thus, the morphology can be optimized by simply varying the temperature conditions. However, precisely control the temperature is still challenging, especially for mass production of large-area devices, thus leading to reproducibility issues. Therefore, there is still room for further improvement in the morphology and photovoltaic performance of OSCs in halogen-free or green solvent process.

In this work, we report the design and synthesis of a novel BDT-free WBG polymer donor, named PDTP-BDD, for realizing efficient green-solvent processed OSCs (**Fig. 1**). PDTP-BDD was developed by bridging dithieno[3,2-b:2′,3′-d]pyridin-5(4H)-one (DTP) donor block and benzo[1,2-c:4,5c′]dithiophene-4,8-dione (BDD) acceptor block with thiophene bridges. As supported by the electrostatic potential calculation results, the electron donating ability of DTP was even lower than thiophene bridge (**Fig. S1**). The weak electron donating ability of DTP makes PDTP-BDD possesses high absorption in the range of 500–700 nm and a HOMO energy

level of −5.45 eV, matching well with those high-performance nonfullerene acceptors (such as L8-BO). These rigid building blocks also make PDTP-BDD has strong aggregation and poor solubility in common halogen-free solvents (such as *o*-xylene) at room temperature, but it is readily dissolved and disaggregated at high temperature (120 °C). After cooling down to a lower temperature (60 °C), PDTP-BDD self-assembled and pre-aggregated slowly in the solution at a long time. To optimize the morphology, layer-by-layer processed OSCs (LbL-OSCs) were fabricated,[16, 44-49] and the morphology of underlying donor layer was optimized by a delayed processing strategy, which was first proposed by our group.[33, 50] By simply varying the delay time, the pre-aggregation of PDTP-BDD in *o*-xylene was successfully controlled, enabling the fibril network optimization and deepening the permeation of acceptor into the donor network. The optimized PDTP-BDD/L8-BO-based LbL-OSCs realized a high PCE of 18.42%. By adding a small amount of D18 to further optimize the PDTP-BDD fibril network, an impressive PCE of 19.36% was achieved finally in the resulting ternary LbL-OSCs, which is the among highest values for OSCs processed by halogen-free solvents.

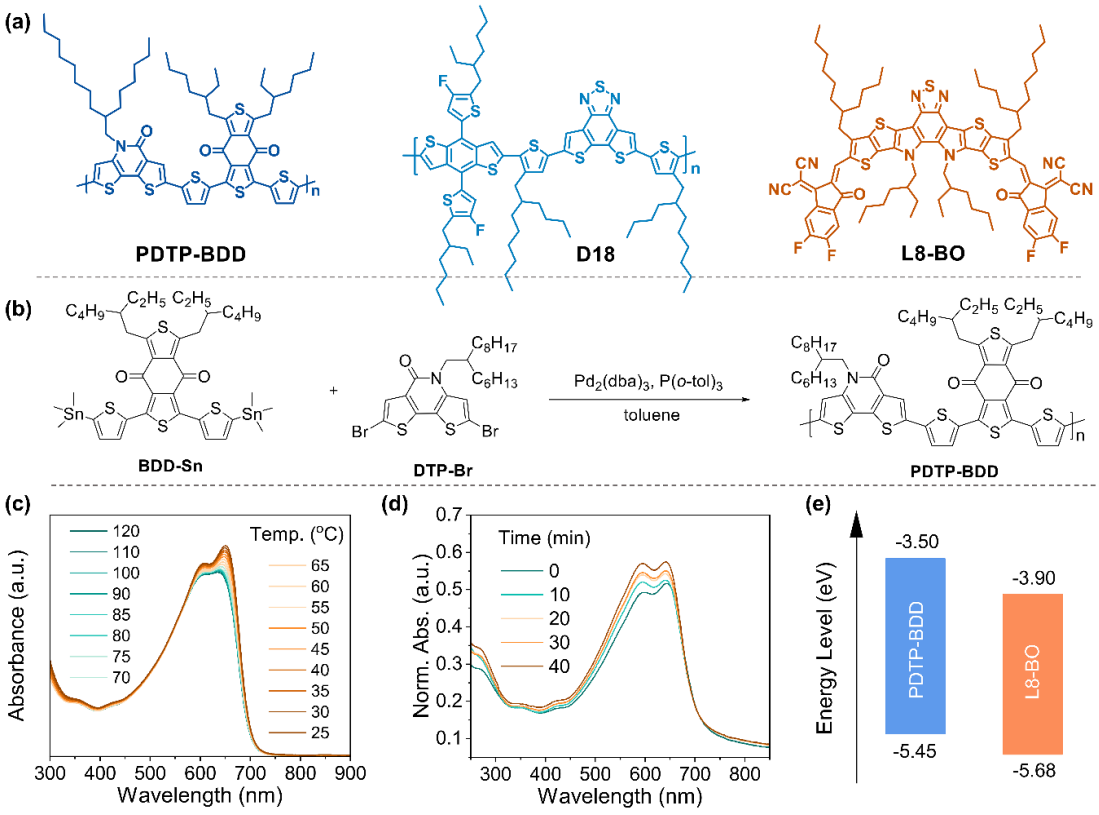

Fig. 1. (a) Chemical structures of PDTP-BDD, D18 and L8-BO. (b) The synthetic route of PDTP-BDD. (c) Temperature-dependent absorption of PDTP-BDD in *o*-xylene solution. (d) UV-vis absorption of PDTP-BDD films processed by different delay times from *o*-xylene solutions (normalized to the film thickness). (e) The energy level diagram of PDTP-BDD and L8-BO.

2. Results and discussion

2.1. Materials synthesis and characterization

PDTP-BDD was synthesized by Stille-coupling of 1,3-bis(2-ethylhexyl)-5,7-bis(5-(trimethylstannyl)thiophen-2-yl)benzo[1,2-c:4,5-c′]dithiophene-4,8-dione (BDD-Sn)[51] with 2,7-dibromo-4-(2-hexyldecyl)dithieno[3,2-*b*:2′,3′-*d*]pyridin-5(4*H*)-one (DTP-Br)[52] in the presence of $Pd_2(dba)_3$/P(*o*-tol) catalyst (**Fig. 1**b and **Fig. S2**). PDTP-BDD exhibited good solubility in common halogenated solvents, such as CF and CB, but poor solubility in halogen-free solvents, such as toluene and *o*-xylene at room temperature. The number-average molecular weight (M_n) and polydispersity index ($Đ$) were determined to be 70.7 kDa and 1.87, respectively, by high-temperature gel chromatography (**Fig. S3**). PDTP-BDD showed good thermal stability with a high decomposition temperature (T_d, 5% weight loss) of 395 °C (**Fig. S4**). No obvious thermal transition was observed in the differential scanning calorimetry (DSC) curve from room temperature up to 350 °C (**Fig. S5**), showing its thermal robustness.

2.2. Optical and electrochemical properties

As PDTP-BDD has poor solubility in *o*-xylene at room temperature, the temperature-dependent absorption was investigated by heating the solution to 120 °C first and then measured during the cooling process (**Fig. 1**c). PDTP-BDD exhibited distinct temperature-dependent absorption with an obvious shoulder peak observed with the temperature below 70 °C, indicating its strong pre-aggregation nature in *o*-xylene. To investigate the pre-aggregation effect on the film-state absorption, the PDTP-BDD solution (10 mg mL^{-1} in *o*-xylene) was

heated up to 120 °C (Step I in **Fig. 2**a), and then kept at 60 °C before film deposition (a delayed processing process, Step II in **Fig. 2**a). The absorption was strengthened with increasing the delayed processing time, indicating the gradual self-assembly of PDTP-BDD during the delayed procedure (Fig. 1d). The optical bandgap (E_g^{opt}) of PDTP-BDD was determined to be 1.75 eV based on the absorption onset. The improved absorption of PDTP-BDD could also be observed in the LbL active layer of PDTP-BDD/L8-BO (**Fig. S6**).

Cyclic voltammetry (CV) experiments were conducted to determine the frontier orbital energy levels (**Fig. S7**). PDTP-BDD had a HOMO of −5.45 eV and a lowest unoccupied molecular orbital (LUMO) energy level of −3.50 eV, corresponding to an electrochemical bandgap (E_g^{CV}) of 1.95 eV. The energy levels matched well with those low bandgap nonfullerene acceptors, such as L8-BO (−5.68/−3.90 eV) (**Fig. 1**e), for achieving high V_{oc} in OSCs.

2.3. Photovoltaic Properties

LbL-OSCs were fabricated and evaluated with a structure of glass/ITO/PEDOT:PSS/PDTP-BDD/L8-BO/PNDIT-F3N/Ag, in which the PDTP-BDD layer was processed with a green-solvent delayed processing procedure (**Fig. 2**a,b). These devices achieved high V_{oc}s up to 0.9 V, and the device performances were sensitive to the delayed processing time of PDTP-BDD in *o*-xylene (**Fig. 2**c and **Table 1**). Without delayed processing treatment, a J_{sc} of 25.18 mA cm^{-2} and FF of 74.68% were obtained, corresponding to a moderate PCE of 17.08%. In comparison, the BHJ-OSCs based on PDTP-BDD:L8-BO (1:1.2 by weight) obtained a lower PCE of 15.90% due to the reduced J_{sc} of 24.24 mA cm^{-2} and FF of 72.60% (**Fig. S8** and **Table S1**). Considering their much lower performance, the BHJ-OSCs were not further investigated in the following studies. For the LbL-OSCs, after delayed processing of PDTP-BDD for 10 min, the J_{sc} and FF were increased to 25.88 mA cm^{-2} and 76.05%, respectively, giving rise to a higher PCE of 17.96%. When the delay time was increased to 20 min, the highest J_{sc} of 26.27 mA cm^{-2} and

FF of 77.19% were realized, which contributed to the highest PCE of 18.42%. Further increasing the delay time to 30 min, slightly decreased J_{sc} of 25.94 mA cm^{-2} and FF of 77.01% were observed, leading to a mildly lower PCE 18.03%. While after delayed for 40 min, the J_{sc} and FF were declined remarkably to 25.48 mA cm^{-2} and 73.17%, respectively, making the PCE sharply decreased to 16.76%. The effect of green-solvent delayed processing on the photovoltaic performance of these LbL-OSCs was also confirmed by external quantum efficiency (EQE) measurements (**Fig. 2**d and **Table 1**). By prolonging the delay time, the EQE response raised at first, then decreased, and the 20 min delayed devices realized the highest EQE response almost throughout the absorption range, giving rise the highest calculated short current density (J_{EQE}) of 25.16 mA cm^{-2}. These results demonstrated green-solvent delayed processing is a useful strategy to improve the performance of LbL-OSCs. Moreover, replacing the L8-BO acceptor with the PY-IT polymer acceptor, an improved PCE from 14.90% to 17.25% could also be obtained (**Fig. S9** and **Table S2**). These results showed the general applicability of PDTP-BDD as polymer donor in OSCs and the application potential of green-solvent delayed processing in improving the performances of LbL-OSCs.

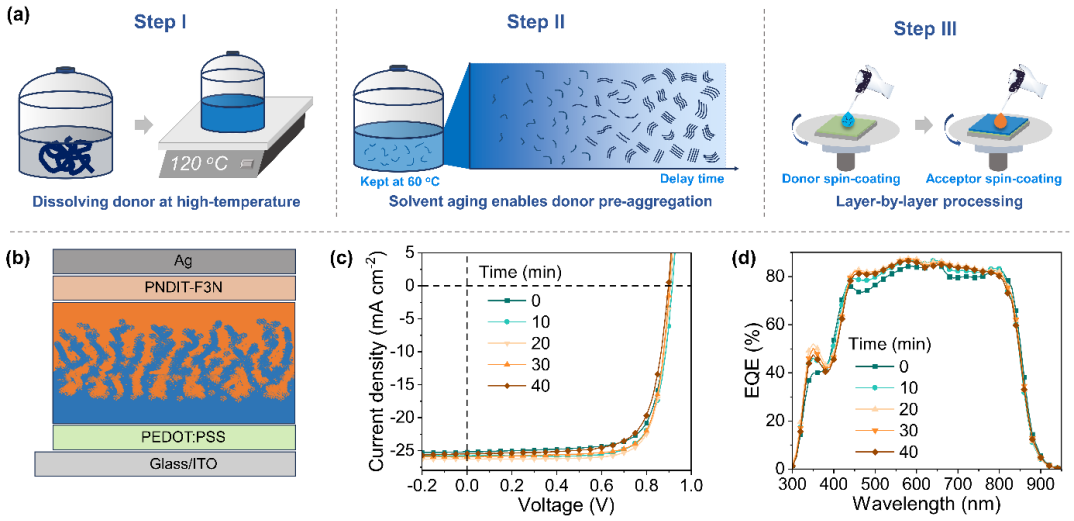

Fig. 2. (a) The schematic illustration of the photoactive layer deposition procedure involving green-solvent delayed processing and LbL processing. (b) The schematic illustration of the device structure of LbL-OSCs. (c) *J-V* curves, and (d) EQE spectra of the PDTP-BDD/L8-BO-based LbL-OSCs prepared by processing PDTP-BDD with different delay times.

Table 1. Photovoltaic parameters of the PDTP-BDD/L8-BO-based LbL-OSCs prepared by processing PDTP-BDD with different delay times.

Delay time (min)	V_{oc} (V)	J_{sc} (mA cm^{-2})	J_{EQE}[b] (mA cm^{-2})	FF (%)	PCE (%)
0	0.908	25.18	24.45	74.68	17.08
	0.909±0.005[a]	24.77±0.30		74.10±0.43	16.69±0.24
10	0.916	25.78	24.80	76.05	17.96
	0.908±0.005	25.71±0.34		75.08±0.71	17.52±0.20
20	0.908	26.27	25.16	77.19	18.42
	0.906±0.005	26.14±0.31		76.93±0.57	18.22±0.25
30	0.903	25.94	24.99	77.01	18.03
	0.900±0.005	25.72±0.22		76.63±0.30	17.75±0.18
40	0.898	25.48	24.77	73.17	16.76
	0.897±0.003	25.45±0.18		72.67±0.74	16.59±0.17

[a] The averaged values with standard deviations were calculated from 20 individual devices. [b] The integrated current densities were calculated from the EQE curves.

2.4. Morphology and charge transport properties

The green-solvent delayed processing effect on the crystallinity and molecular packing behaviors of PDTP-BDD and PDTP-BDD/L8-BO films were studied by grazing incidence wide angle X-ray scattering (GIWAXS) measurements (**Fig. 3** and **Fig. S10**). Without delayed processing treatment, the PDTP-BDD film exhibited a (100) diffraction peak at q_{xy} = 2.39 nm^{-1}, corresponding to the lamellar stacking distance (d_l) of 2.68 nm (**Table S3**). After delayed processing, the d_l was decreased to 2.57 nm (q_{xy} = 2.44 nm^{-1}), indicating the more compacted lamellar packing. The crystal coherence lengths (CCLs) of their lamellar stacking were estimated to be 6.49, 6.80 and 7.03 nm for PDTP-BDD films processed from 0, 20, and 40 min delayed solutions, respectively. All these films exhibited well-defined (010) diffractions at q_z = 17.3 nm^{-1} in the out-of-plane direction, corresponding to their π-π stacking distance (d_π) of 0.363 nm. The CCLs of their π-π stacking were estimated to be 2.82, 3.06, and 3.14 nm for PDTP-BDD films processed from 0, 20, and 40 min delayed solutions, respectively. The results indicated the intensified molecular packing of PDTP-BDD induced by delayed processing

possess. The improved molecular packing order could be preserved after deposing L8-BO on top of the PDTP-BDD layer. As PDTP-BDD and L8-BO had very closed lamellar and π-π stacking peaks (around 17.5 nm^{-1}), it was difficult to divide them from each other in the PDTP-BDD/L8-BO films. Thus, only the lamellar stackings of the PDTP-BDD/L8-BO films were analyzed and summarized in Table S3. It was worth noting that the 40 min delayed PDTP-BDD/L8-BO film appeared new peaks compared to other films, which indicated that a long-time delayed processing might lead to different packing behaviors.

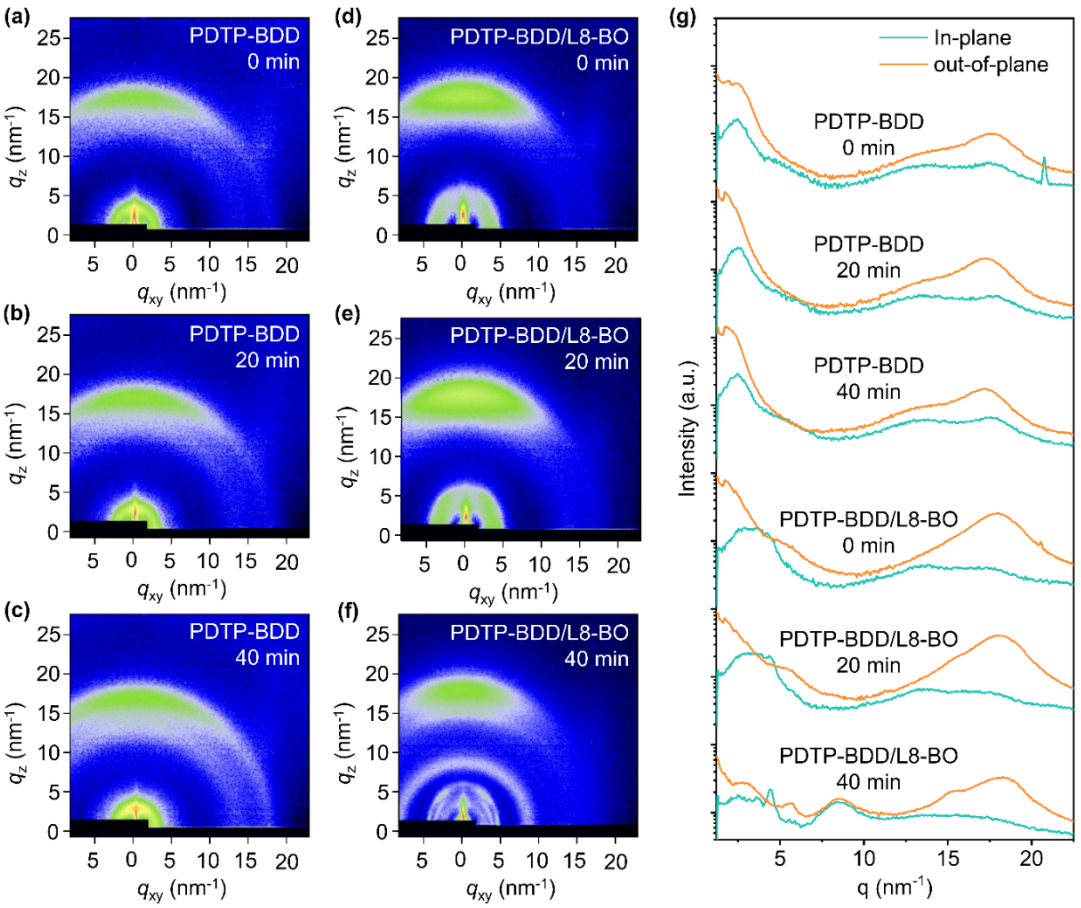

Fig. 3. (a-f) GIWAXS images of the PDTP-BDD and PDTP-BDD/L8-BO thin films prepared by processing PDTP-BDD with different delay times. (g) In-plane and out-of-plane line-cuts from (a-f).

The effect of green green-solvent delayed processing on the morphology of PDTP-BDD was also investigated by atomic force microscopy (AFM) measurements (**Fig. 4**a-f). Without delayed processing treatment, the PDTP-BDD film exhibited a quite smooth top surface with a small root mean square roughness (R_q) of 0.911 nm. Very small fibrils compactly distributed

throughout the phase image, which was not favorable for acceptor permeation deep into the donor matrix. Fortunately, both the lengths and widths of PDTP-BDD fibrils increased significantly after delayed for 20 min, and resulting in a slightly increased R_q of 1.01 nm. Such a well-defined nano fibrous network of PDTP-BDD was beneficial for higher charge carrier transport. More important, the L8-BO acceptor could permeate more readily deep into the fibril mesh of PDTP-BDD, providing a better vertical phase separation with sufficient D/A interfaces for more efficient charge separation. Prolonging the delay time to 40 min, the over aggregated PDTP-BDD fibrils were observed in the AFM images, which led to a much larger R_q of 2.20 nm. The large aggregates not only reduced the D/A interfaces but also served as morphological traps hindering the charge extraction.

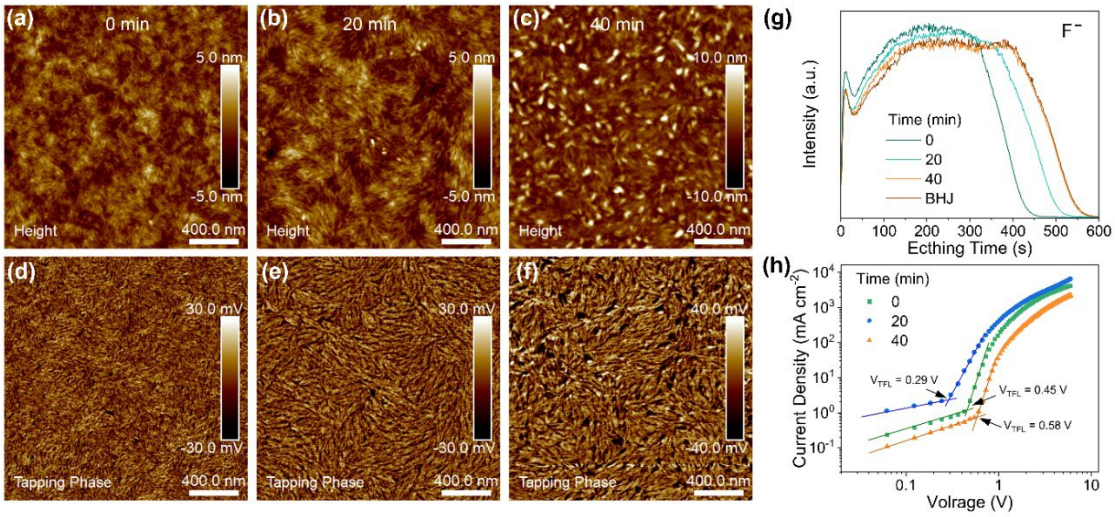

Fig. 4. AFM (a-c) height images and (d-f) phase images of the PDTP-BDD thin films processed from *o*-xylene solutions with different delay times. (g) TOF-SIMS spectra of the control BHJ blend (PDTP-BDD:L8-BO) and the LbL films (PDTP-BDD/L8-BO) prepared by processing PDTP-BDD with different delay times. (h) *J*-*V* curves of the ITO/PEDOT:PSS/PDTP-BDD/MoO_3/Ag devices prepared by processing PDTP-BDD with different delay times.

The green-solvent delayed processing effect on the vertical phase separation was studied by time-of-flight secondary ion mass spectrometry (TOF-SIMS) measurements (**Fig. 4**g). The F^- signals were monitored to denote the vertical distribution of L8-BO in the active layer. The BHJ blend of PDTP-BDD:L8-BO (1:1.2 by weight) was also measured as a reference, and all the

films were kept at the same thickness. The rising stage of F^- signals was due to signal delay as the etching started.[30] Without delayed processing, the LbL film of PDTP-BDD/L8-BO exhibited higher intensity of F^- signals at early etching stage, but declined much earlier than the control BHJ blend. With increasing the delay time, lower intensities of F^- were observed, but it also needed longer etching time to fully remove the signals. When the delay time reaching 40 min, the F^- profiles showed almost the same to that of the control BHJ film. The results demonstrated that the green-solvent delayed processing could promote the permeation of L8-BO into the fibril mesh of PDTP-BDD, and the depth could be controlled by just varying the delay time (**Fig. 1**b). The main reason was that the green-solvent delayed processing enabled the pre-aggregation and fibrils formation, which resulted in less compact stacking of fibrils (more space between fibrils), thus favoring the permeation of acceptor molecule deep into the donor layer. For the control LbL active layer, the more compact packing of PDTP-BDD maded L8-BO mainly located on the top surface of the active layer, which was more like a bilayer structure. With the delay time increasing, the fibrillization of PDTP-BDD made the donor layer had more and larger interspaces between fibril matrixes and allowed the L8-BO acceptor to fill into these interspaces and penetrated in depth into the active layer. As a result, a more favorable vertical component deposition was realized by just tuning the delayed processing time.

The green-solvent delayed processing effect on the charge transport properties of PDTP-BDD film was studied by the space charge limited current (SCLC) method (**Fig. 4**h and **Table S4**). The J-V curves showed typically three regions, Ohmic contact, trap-filled limit as well as SCLC current regions at low, middle and higher voltage biases, respectively. The V_{TFL} (a voltage determined by the cross crosspoint of Ohmic contact and trap-filled limit region) was 0.45, 0.29 and 0.58 V for the 0, 20 and 40 min delayed PDTP-BDD films, and their trap densities were estimated to be 1.5×10^{16}, 0.96×10^{16}, 1.9×10^{16} cm^{-3}, respectively. In addition, the hole mobilities were estimated to be 1.4×10^{-3}, 2.2×10^{-3}, 8.6×10^{-4}, $cm^2\ V^{-1}\ s^{-1}$ for the 0, 20

and 40 min delayed PDTP-BDD films, respectively. The lower trap density and higher hole mobility of the 20 min delayed PDTP-BDD film could be beneficial for more efficient charge transport and suppressed charge recombination in devices.

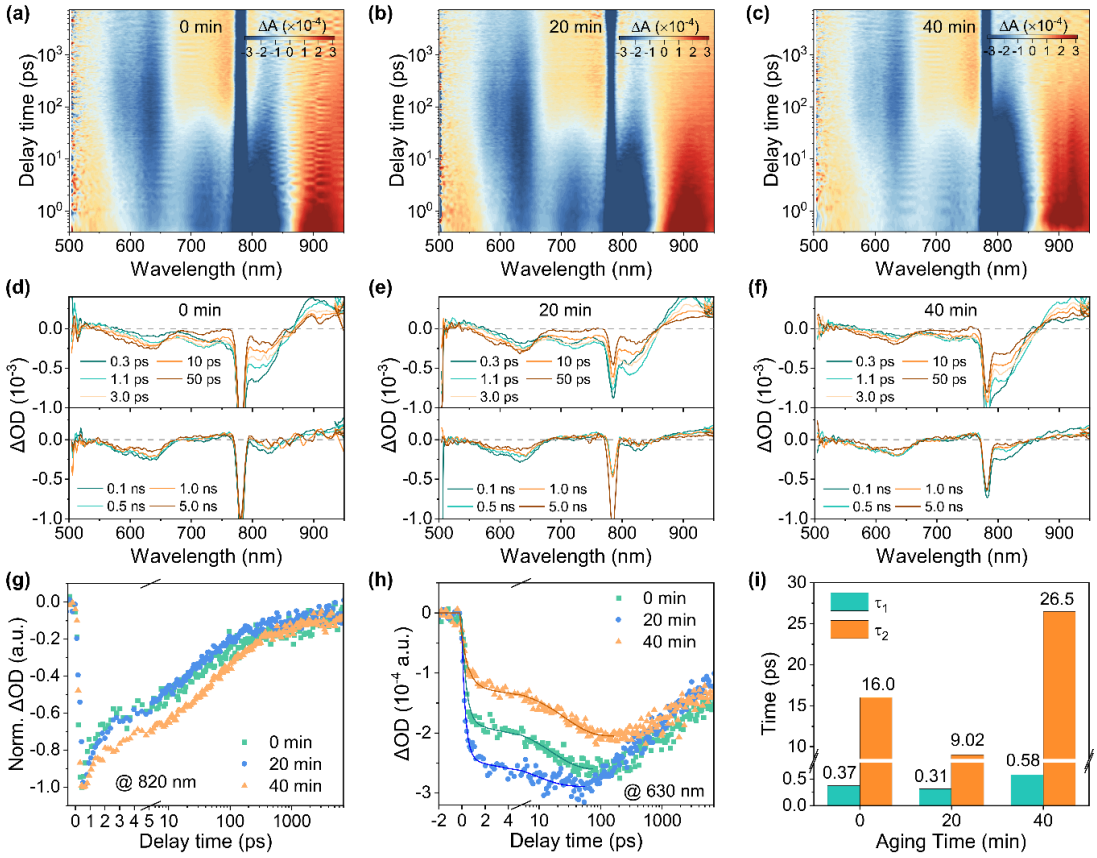

Fig. 5. (a-c) 2D color plots of fs-TA spectra of the PDTP-BDD/L8-BO films prepared by processing PDTP-BDD with different delay times. (d-f) The corresponding TA spectra of the PDTP-BDD/L8-BO films. (g) TA kinetics of the GSB signals at 820 nm. (h) TA kinetics of the GSB signals at 630 nm. (i) The hole transfer times estimated from fitting the TA kinetics.

2.5. Charge transfer dynamics

Femtosecond transient absorption spectroscopy (fs-TAS) was used to study the effect of green-solvent delayed processing on the charge transfer dynamics (**Fig. 5**). A 780 nm excitation was used to excite L8-BO only, however, PDTP-BDD had no absorption in such wavelength. The immediately decay traces around 820 and 900 nm were assigned to the ground-state bleach (GSB) of L8-BO and excited-state absorption (ESA), respectively.[30] The signal raised first then decayed around 630 nm was assigned to the GSB of PDTP-BDD, suggesting the hole-

transfer from L8-BO to PDTP-BDD. The 20 min delayed film exhibited faster GSB decay at 820 nm and much stronger GSB signals at 630 nm than the other conditions, indicating the more efficient hole transfer of the former (**Fig. 5**g,h). By biexponentially fitting the GSB signals at 630 nm, the charge transfer lifetimes were quantified by two components, where a fast component τ_1 was assigned to interfacial hole-transfer process and the second component τ_2 represented the diffusion-limited dissociation of bulk excitons.[6] The τ_1/τ_2 were estimated to be 0.37/16.0, 0.31/9.02 and 0.58/26.5 ps for 0, 20 and 40 min delayed films, respectively (**Fig. 5**i). The smaller τ_1/τ_2 of 20 min delayed PDTP-BDD/L8-BO film suggested the faster hole transfer in the corresponding devices, which agreed well with the more efficient hole transfer. The results explained why the 20 min delayed devices could achieve higher photovoltaic performances.

2.6. Applications in ternary LbL-OSCs

The application potential of green-solvent delayed processing in the ternary blend LbL-OSCs was investigated by adding D18 as a second donor for it has stronger aggregation tendency and complementary absorption with PDTP-BDD (**Fig. 6**a). The addition of a small amount of D18 (20 wt% relative to the total donor) resulted in the further optimized fibrillar structure of the PDTP-BDD:D18 blend (**Fig. S11**). Further adding D18 into the PDTP-BDD:D18 blend led to fast aggregation of the donors and smaller fibrils in the thin films, due to the poor solubility of D18 in *o*-xylene. Such morphology evolution agreed well with the photovoltaic performance variation trend in the corresponding ternary blend LbL-OSCs (**Fig. 6**b-e and **Table S5**). With 20 wt% D18 added, the J_{sc} and FF were significantly improved to 26.90 mA cm^{-2} and 79.53%, respectively, thus contributing to a champion PCE of 19.36%. This is among the highest values for OSCs processed by halogen-free solvents (**Fig. 6**f and **Table S6**). While adding D18 more than 20wt%, the sharply decreased PCEs were observed, due to the poor solubility of D18 making it difficult to control the morphology. The results

demonstrated that the green-solvent delayed processing strategy could also be expanded to the ternary blend LbL-OSCs for further improving the device performances.

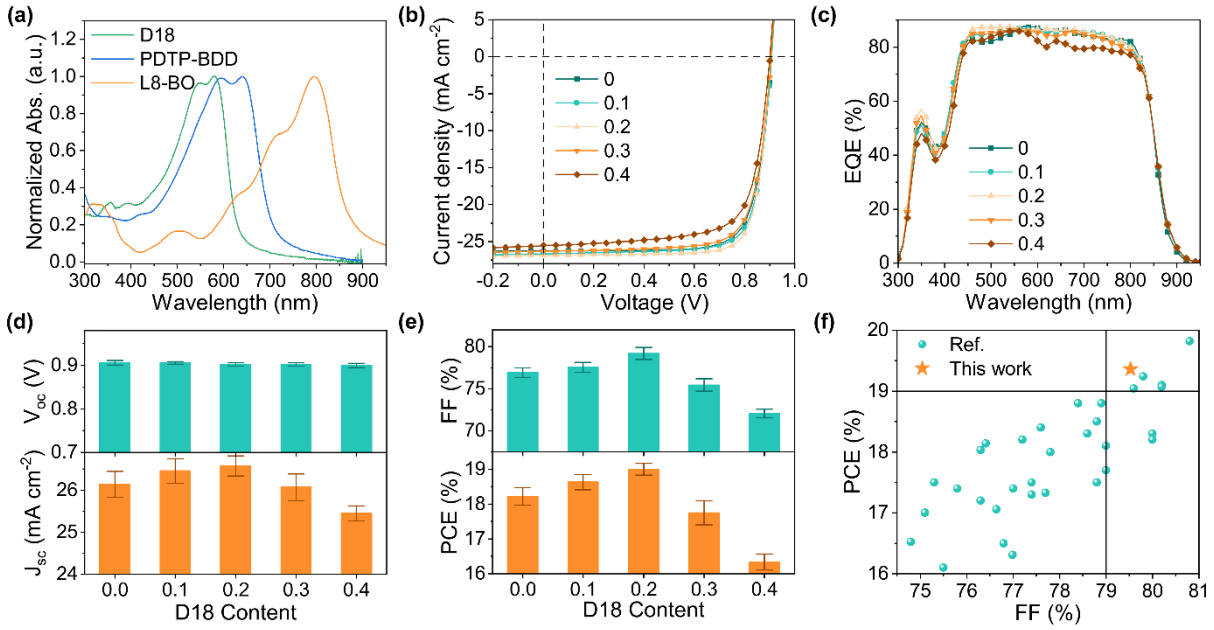

Fig. 6. (a) UV-vis absorption of D18, PDTP-BDD and L8-BO films. (b) *J*-*V* curves, (c) EQE spectra, (d) Column plots of V_{oc} and J_{sc} distributions, and (e) Column plots of FF and PCE distributions of the ternary LbL-OSCs based on PDTP-BDD:D18/L8-BO with various D18 ratios in the donor layer. (f) Summarized PCE versus FF plots of the OSCs processed by halogen-free solvents.

3. Conclusions

In summary, we presented here the design and synthesis of a novel BDT-free D-A copolymer, named PDTP-BDD, and investigated its application as an electron donor for green-solvent processed high-performance OSCs. The combination of two acceptor blocks, BDD and DTP, made the polymer possessed an E_g^{opt} of 1.75 eV and a HOMO level of −5.45 eV. The high planar structure of PDTP-BDD resulted in strong aggregation and poor solubility in the halogen-free solvent of *o*-xylene at room temperature, but it was dissolved well and disaggregated at 120 °C. After cooling down to 60 °C, PDTP-BDD self-assembled and pre-aggregated slowly in *o*-xylene at a long-time. By simply varying the delayed processing time, the pre-aggregation of PDTP-BDD in *o*-xylene was successfully controlled, enabling the fibril

network optimization and deepening the permeation of acceptor into the donor network in the LbL-OSCs. The optimized PDTP-BDD/L8-BO-based LbL-OSCs realized a high PCE of 18.42%. Moreover, by adding 20wt% of D18 to further optimize the PDTP-BDD fibril network during delayed processing, an impressive PCE of 19.36% was achieved finally in the resulting ternary blend LbL-OSCs. Overall, our research provides a guideline of high-performance polymer donor design and device engineering to realize more efficient OSCs processed by green solvents.

Declaration of Competing Interest

The authors declare that they have no known competing financial interests or personal relationships that could have appeared to influence the work reported in this paper.

Acknowledgements

This work was financially supported by the National Key Research and Development Program of China (Grant No. 2022YFB4200500), National Natural Science Foundation of China (NSFC, 21825502, 22075190, 22105135 and 22379101), Sichuan Natural Science Foundation (2023NSFSC0304 and 24ZNSFSC0030), Special Fund for Strategic Cooperation Between Sichuan University and Suining City (2022CDSN-01), and Special Fund for Strategic Cooperation Between Sichuan University and Dazhou City (2022CDDZ-04). The authors thank Yanping Huang from Center of Engineering Experimental Teaching, School of Chemical Engineering, Sichuan University for the help of NMR measurements. The authors also thank National Synchrotron Light Source II (NSLS-II, Contract No. DE-SC0012704) Brookhaven National Laboratory for providing GIWAXS experiment time.

Appendix A. Supplementary data

Supplementary data to this article can be found online at XX.

References

[1] C. Liu, L. Shao, S. Chen, Z. Hu, H. Cai, F. Huang. Recent progress in π-conjugated polymers for organic photovoltaics: Solar cells and photodetectors. Prog. Polym. Sci. 143 (2023) 101711, https://doi.org/10.1016/j.progpolymsci.2023.101711.

[2] X. Yang, Y. Shao, S. Wang, M. Chen, B. Xiao, R. Sun, J. Min. Processability considerations for next‐generation organic photovoltaic materials. Adv. Mater. 36 (2024) 2307863, https://doi.org/10.1002/adma.202307863.

[3] H. Yao, J. Wang, Y. Xu, S. Zhang, J. Hou. Recent progress in chlorinated organic photovoltaic materials. Acc. Chem. Res. 53 (2020) 822-832, https://doi.org/10.1021/acs.accounts.0c00009.

[4] Q. Wu, Y. Yu, X. Xia, Y. Gao, T. Wang, R. Sun, J. Guo, S. Wang, G. Xie, X. Lu, E. Zhou, J. Min. High-performance organic photovoltaic modules using eco-friendly solvents for various indoor application scenarios. Joule 6 (2022) 2138-2151, https://doi.org/10.1016/j.joule.2022.07.001.

[5] X. Chen, Y. Li, W. Jin, T. Zhou, X. Xu, Y. Duan, L. Yu, R. Li, Q. Peng. Layer-by-layer organic solar cells enabled by 1, 2, 4-selenadiazole-containing crystalline small molecule with double-fibril network morphology. Angew. Chem. Int. Ed. 63 (2024) e202402831, https://www.ncbi.nlm.nih.gov/pubmed/38532290.

[6] P. Wu, Y. Duan, Y. Li, X. Xu, R. Li, L. Yu, Q. Peng. 18.6% efficiency all‐polymer solar cells enabled by a wide bandgap polymer donor based on benzo[1,2‐d:4,5‐d′]bisthiazole. Adv. Mater. 36 (2024) 2306990, https://doi.org/10.1002/adma.202306990.

[7] B. Pang, C. Liao, X. Xu, S. Peng, J. Xia, Y. Guo, Y. Xie, Y. Chen, C. Duan, H. Wu, R. Li, Q. Peng. B-n bond embedded triplet terpolymers with small singlet-triplet energy gaps for suppressing non-radiative recombination and improving blend morphology in organic solar cells. Adv. Mater. 35 (2023) 2211871, https://doi.org/10.1002/adma.202211871.

[8] G. Wu, X. Xu, C. Liao, L. Yu, R. Li, Q. Peng. Improving cooperative interactions between halogenated aromatic additives and aromatic side chain acceptors for realizing 19.22% efficiency polymer solar cells. Small 19 (2023) 2302127, https://doi.org/10.1002/smll.202302127.

[9] K. Liu, Y. Jiang, F. Liu, G. Ran, F. Huang, W. Wang, W. Zhang, C. Zhang, J. Hou, X. Zhu. Organic solar cells with over 19% efficiency enabled by a 2d-conjugated non-fullerene acceptor featuring favorable electronic and aggregation structures. Adv. Mater. 35 (2023) 2300363, https://doi.org/10.1002/adma.202300363.

[10] Q. Fan, R. Ma, Z. Bi, X. Liao, B. Wu, S. Zhang, W. Su, J. Fang, C. Zhao, C. Yan, K. Chen, Y. Li, C. Gao, G. Li, W. Ma. 19.28% efficiency and stable polymer solar cells enabled by introducing an nir‐absorbing guest acceptor. Adv. Funct. Mater. 33 (2023) 2211385, https://doi.org/10.1002/adfm.202211385.

[11] M. Deng, X. Xu, Y. Duan, L. Yu, R. Li, Q. Peng. Y-type non-fullerene acceptors with outer branched side chains and inner cyclohexane side chains for 19.36% efficiency polymer solar cells. Adv. Mater. 35 (2023) 2210760, https://doi.org/10.1002/adma.202210760.

[12] M. Deng, X. Xu, Y. Duan, W. Qiu, L. Yu, R. Li, Q. Peng. 19.32% efficiency polymer solar cells enabled by fine-tuning stacking modes of y-type molecule acceptors: Synergistic bromine and fluorine substitution of the end groups. Adv. Mater. 36 (2024) 2308216, https://doi.org/10.1002/adma.202308216.

[13] T. Chen, S. Li, Y. Li, Z. Chen, H. Wu, Y. Lin, Y. Gao, M. Wang, G. Ding, J. Min, Z. Ma, H. Zhu, L. Zuo, H. Chen. Compromising charge generation and recombination of organic photovoltaics with mixed diluent strategy for certified 19.4% efficiency. Adv. Mater. 35 (2023) 2300400, https://doi.org/10.1002/adma.202300400.

[14] L. Zhu, M. Zhang, J. Xu, C. Li, J. Yan, G. Zhou, W. Zhong, T. Hao, J. Song, X. Xue, Z. Zhou, R. Zeng, H. Zhu, C.C. Chen, R.C.I. MacKenzie, Y. Zou, J. Nelson, Y. Zhang, Y. Sun, F. Liu. Single-junction organic solar cells with over 19% efficiency enabled by a refined double-fibril network morphology. Nat. Mater. 21 (2022) 656-663, https://doi.org/10.1038/s41563-022-01244-y.

[15] J. Wang, Y. Wang, P. Bi, Z. Chen, J. Qiao, J. Li, W. Wang, Z. Zheng, S. Zhang, X. Hao, J. Hou. Binary organic solar cells with 19.2% efficiency enabled by solid additive. Adv. Mater. 35 (2023) 2301583, https://doi.org/10.1002/adma.202301583.

[16] K. Chong, X. Xu, H. Meng, J. Xue, L. Yu, W. Ma, Q. Peng. Realizing 19.05% efficiency polymer solar cells by progressively improving charge extraction and suppressing charge recombination. Adv. Mater. 34 (2022) 2109516, https://doi.org/10.1002/adma.202109516.

[17] T. Xu, Z. Luo, R. Ma, Z. Chen, T.A. Dela Pena, H. Liu, Q. Wei, M. Li, C. Zhang, J. Wu, X. Lu, G. Li, C. Yang. High-performance organic solar cells containing pyrido[2,3-b]quinoxaline-core-based small-molecule acceptors with optimized orbit overlap lengths and molecular packing. Angew. Chem. Int. Ed. 62 (2023) e202304127, https://www.ncbi.nlm.nih.gov/pubmed/37232174.

[18] W. Wei, C.e. Zhang, Z. Chen, W. Chen, G. Ran, G. Pan, W. Zhang, P. Müller-Buschbaum, Z. Bo, C. Yang, Z. Luo. Precise methylation yields acceptor with hydrogen-bonding network for high-efficiency and thermally stable polymer solar cells. Angew. Chem. Int. Ed. 63 (2024) e202315625, https://doi.org/10.1002/anie.202315625.

[19] X. Xu, X. Yuan, Q. Fan, C. Duan, M. Zhang, Q. Peng. Conjugated polymer donors for organic solar cells [M]. Organic solar cells: Materials design, technology and commercialization. 2022: 1-76.

[20] Z.a. Li, C.-C. Chueh, A.K.Y. Jen. Recent advances in molecular design of functional conjugated polymers for high-performance polymer solar cells. Prog. Polym. Sci. 99 (2019) 101175, https://doi.org/10.1016/j.progpolymsci.2019.101175.

[21] M.J. Zhang, X. Guo, W. Ma, H. Ade, J.H. Hou. A large-bandgap conjugated polymer for versatile photovoltaic applications with high performance. Adv. Mater. 27 (2015) 4655-4660, https://doi.org/10.1002/adma.201502110.

[22] Q. Liu, Y. Jiang, K. Jin, J. Qin, J. Xu, W. Li, J. Xiong, J. Liu, Z. Xiao, K. Sun, S. Yang, X. Zhang, L. Ding. 18% efficiency organic solar cells. Sci. Bull. 65 (2020) 272-275, https://doi.org/10.1016/j.scib.2020.01.001.

[23] B. Pang, C. Liao, X. Xu, L. Yu, R. Li, Q. Peng. Benzo[d]thiazole based wide bandgap donor polymers enable 19.54% efficiency organic solar cells along with desirable batch-to-batch reproducibility and general applicability. Adv. Mater. 35 (2023) 2300631, https://doi.org/10.1002/adma.202300631.

[24] C.K. Sun, F. Pan, H.J. Bin, J.Q. Zhang, L.W. Xue, B.B. Qiu, Z.X. Wei, Z.G. Zhang, Y.F. Li. A low cost and high performance polymer donor material for polymer solar cells. Nat. Commun. 9 (2018) 743, https://doi.org/10.1038/s41467-018-03207-x.

[25] Z. Wang, X. Wang, L. Tu, H. Wang, M. Du, T. Dai, Q. Guo, Y. Shi, E. Zhou. Dithienoquinoxalineimide-based polymer donor enables all-polymer solar cells over 19% efficiency. Angew. Chem. Int. Ed. 63 (2024) e202319755, https://doi.org/10.1002/anie.202319755.

[26] H. Yao, L. Ye, H. Zhang, S. Li, S. Zhang, J. Hou. Molecular design of benzodithiophene-based organic photovoltaic materials. Chem. Rev. 116 (2016) 7397-7457, https://doi.org/10.1021/acs.chemrev.6b00176.

[27] B. Zheng, L.J. Huo, Y.F. Li. Benzodithiophenedione-based polymers: Recent advances in organic photovoltaics. NPG Asia Mater. 12 (2020) 3, https://doi.org/10.1038/s41427-019-0163-5.

[28] A.J. Heeger. 25th anniversary article: Bulk heterojunction solar cells: Understanding the mechanism of operation. Adv. Mater. 26 (2014) 10-27, https://doi.org/10.1002/adma.201304373.

[29] X. Xu, Y. Li, Q. Peng. Ternary blend organic solar cells: Understanding the morphology from recent progress. Adv. Mater. 34 (2022) 2107476, https://doi.org/10.1002/adma.202107476.

[30] X. Xu, W. Jing, H. Meng, Y. Guo, L. Yu, R. Li, Q. Peng. Sequential deposition of multicomponent bulk heterojunctions increases efficiency of organic solar cells. Adv. Mater. 35 (2023) 2208997, https://doi.org/10.1002/adma.202208997.

[31] Y. Ran, C. Liang, Z. Xu, W. Jing, X. Xu, Y. Duan, R. Li, L. Yu, Q. Peng. Developing efficient benzene additives for 19.43% efficiency of organic solar cells by crossbreeding effect of fluorination and bromination. Adv. Funct. Mater. 34 (2024) 2311512, https://doi.org/10.1002/adfm.202311512.

[32] F.W. Zhao, C.R. Wang, X.W. Zhan. Morphology control in organic solar cells. Adv. Energy Mater. 8 (2018) 1703147, https://doi.org/10.1002/aenm.201703147.

[33] X. Xu, L. Yu, H. Yan, R. Li, Q. Peng. Highly efficient non-fullerene oganic solar cells enabled by a delayed processing method using a non-halogenated solvent. Energy Environ. Sci. 13 (2020) 4381-4388, https://doi.org/10.1039/d0ee02034f.

[34] X. Wu, X. Jiang, X. Li, J. Zhang, K. Ding, H. Zhuo, J. Guo, J. Li, L. Meng, H. Ade, Y. Li. Introducing phenyl end group in the inner side chains of a-da'd-a acceptors enables high-efficiency organic solar cells processed with nonhalogenated solvent. Adv. Mater. 35 (2023) 2302946, https://doi.org/10.1002/adma.202302946.

[35] J. Xue, H. Zhao, B. Lin, Y. Wang, Q. Zhu, G. Lu, B. Wu, Z. Bi, X. Zhou, C. Zhao, G. Lu, K. Zhou, W. Ma. Nonhalogenated dual-slot-die processing enables high-efficiency organic solar cells. Adv. Mater. 34 (2022) e2202659, https://doi.org/10.1002/adma.202202659.

[36] Y. Zhang, K. Liu, J. Huang, X. Xia, J. Cao, G. Zhao, P.W.K. Fong, Y. Zhu, F. Yan, Y. Yang, X. Lu, G. Li. Graded bulk-heterojunction enables 17% binary organic solar cells via nonhalogenated open air coating. Nat. Commun. 12 (2021) 4815, https://doi.org/10.1038/s41467-021-25148-8.

[37] S. Luo, C. Li, J. Zhang, X. Zou, H. Zhao, K. Ding, H. Huang, J. Song, J. Yi, H. Yu, K.S. Wong, G. Zhang, H. Ade, W. Ma, H. Hu, Y. Sun, H. Yan. Auxiliary sequential deposition enables 19%-efficiency organic solar cells processed from halogen-free

solvents. Nat. Commun. 14 (2023) 6964, https://dx.doi.org/10.1038/s41467-023-41978-0.

[38] J. Wan, L. Zeng, X. Liao, Z. Chen, S. Liu, P. Zhu, H. Zhu, Y. Chen. All-green solvent‐processed planar heterojunction organic solar cells with outstanding power conversion efficiency of 16%. Adv. Funct. Mater. 32 (2021) 2107567, https://doi.org/10.1002/adfm.202107567.

[39] S. Li, H. Zhang, S. Yue, X. Yu, H. Zhou. Recent advances in non-fullerene organic photovoltaics enabled by green solvent processing. Nanotechnology 33 (2021) 072002, https://doi.org/10.1088/1361-6528/ac020b.

[40] X. Xu, T. Yu, Z. Bi, W. Ma, Y. Li, Q. Peng. Realizing over 13% efficiency in green-solvent-processed nonfullerene organic solar cells enabled by 1,3,4-thiadiazole-based wide-bandgap copolymers. Adv. Mater. 30 (2018) 1703973, https://doi.org/10.1002/adma.201703973.

[41] H. Li, S. Liu, X. Wu, S. Yao, X. Hu, Y. Chen. Advances in the device design and printing technology for eco-friendly organic photovoltaics. Energy Environ. Sci. 16 (2023) 76-88, https://doi.org/10.1039/d2ee03246e.

[42] J.B. Zhao, Y.K. Li, G.F. Yang, K. Jiang, H.R. Lin, H. Ade, W. Ma, H. Yan. Efficient organic solar cells processed from hydrocarbon solvents. Nat. Energy 1 (2016) 15027, https://doi.org/10.1038/Nenergy.2015.27.

[43] D. Wang, G.Q. Zhou, Y.H. Li, K.R. Yan, L.L. Zhan, H.M. Zhu, X.H. Lu, H.Z. Chen, C.Z. Li. High-performance organic solar cells from non-halogenated solvents. Adv. Funct. Mater. 32 (2021) 2107827, https://doi.org/10.1002/adfm.202107827.

[44] K. Weng, L. Ye, L. Zhu, J. Xu, J. Zhou, X. Feng, G. Lu, S. Tan, F. Liu, Y. Sun. Optimized active layer morphology toward efficient and polymer batch insensitive organic solar cells. Nat. Commun. 11 (2020) 2855, https://doi.org/10.1038/s41467-020-16621-x.

[45] R. Yu, X. Wei, G. Wu, Z. Tan. Layer‐by‐layered organic solar cells: Morphology optimizing strategies and processing techniques. Aggregate 3 (2021) e107, https://doi.org/10.1002/agt2.107.

[46] W. Gao, F. Qi, Z. Peng, F.R. Lin, K. Jiang, C. Zhong, W. Kaminsky, Z. Guan, C.S. Lee, T.J. Marks, H. Ade, A.K. Jen. Achieving 19% power conversion efficiency in planar-mixed heterojunction organic solar cells using a pseudosymmetric electron acceptor. Adv. Mater. 34 (2022) 2202089, https://doi.org/10.1002/adma.202202089.

[47] M. Zhou, C. Liao, Y. Duan, X. Xu, L. Yu, R. Li, Q. Peng. 19.10% efficiency and 80.5% fill factor layer-by-layer organic solar cells realized by 4-bis(2-thienyl)pyrrole-2,5-dione based polymer additives for inducing vertical segregation morphology. Adv. Mater. 35 (2023) 2208279, https://doi.org/10.1002/adma.202208279.

[48] L. Wang, C. Chen, Y.W. Fu, C.H. Guo, D.H. Li, J.C. Cheng, W. Sun, Z.R. Gan, Y.D. Sun, B.J. Zhou, C.H. Liu, D. Liu, W. Li, T. Wang. Donor-acceptor mutually diluted heterojunctions for layer-by-layer fabrication of high-performance organic solar cells. Nat. Energy 9 (2024) 208-218, https://doi.org/10.1038/s41560-023-01436-z.

[49] Y. Wei, Z. Chen, G. Lu, N. Yu, C. Li, J. Gao, X. Gu, X. Hao, G. Lu, Z. Tang, J. Zhang, Z. Wei, X. Zhang, H. Huang. Binary organic solar cells breaking 19% via manipulating the vertical component distribution. Adv. Mater. 34 (2022) 2204718, https://doi.org/10.1002/adma.202204718.

[50] X. Xu, G. Zhang, L. Yu, R. Li, Q. Peng. P3ht-based polymer solar cells with 8.25% efficiency enabled by a matched molecular acceptor and smart green-solvent processing technology. Adv. Mater. 31 (2019) 1906045, https://doi.org/10.1002/adma.201906045.

[51] H. Zhang, S. Zhang, K. Gao, F. Liu, H. Yao, B. Yang, C. He, T.P. Russell, J. Hou. Low band-gap conjugated polymer based on diketopyrrolopyrrole units and its application in organic photovoltaic cells. J. Mater. Chem. A 5 (2017) 10416-10423, https://doi.org/10.1039/c7ta01250k.

[52] M. An, F. Xie, X. Geng, J. Zhang, J. Jiang, Z. Lei, D. He, Z. Xiao, L. Ding. A high-performance d-a copolymer based on dithieno[3,2-b:2′,3′-d]pyridin-5(4h)-one unit compatible with fullerene and nonfullerene acceptors in solar cells. Adv. Energy Mater. 7 (2017) 1602509, https://doi.org/10.1002/aenm.201602509.